Determination of the moments of the proton charge density

M. Atoui [1], M. B. Barbaro [2,3] M. Hoballah,[1] C. Keyrouz [1,4] M. Lassaut,[1] D. Marchand,[1]
G. Quéméner [5], and E. Voutier[1]

[1] *Université Paris-Saclay, CNRS/IN2P3, IJCLab*, 91405 Orsay, France
[2] *Dipartimento di Fisica, Universitá di Torino and INFN Sezione di Torino*, 10125 Torino, Italy
[3] *IPSA-DRII*, 94200 Ivry-sur-Seine, France
[4] *Université Côte d'Azur, Institut de Physique de Nice*, 06200 Nice, France
[5] *Normandie Université*, ENSICAEN, UNICAEN, CNRS/IN2P3, *LPC Caen*, 14000 Caen, France

A global analysis of proton electric form factor experimental data from Rosenbluth separation and low squared four-momentum transfer experiments is discussed for the evaluation of the spatial moments of the proton charge density based on the recently published integral method [Hoballah *et al.*, Phys. Lett. B **808**, 135669 (2020)]. Specific attention is paid to the evaluation of the systematic errors of the method, particularly the sensitivity to the choice of the mathematical expression of the form factor fitting function. Within this comprehensive analysis of proton electric form factor data, the moments of the proton charge density are determined for integer order moments, particularly: $\langle r^2 \rangle = 0.694(09)_{\text{stat}}(16)_{\text{sys}}$ fm^2, $\langle r^3 \rangle = 0.870(46)_{\text{stat}}(80)_{\text{sys}}$ fm^3, and $\langle r^4 \rangle = 1.47(25)_{\text{stat}}(45)_{\text{stat}}$ fm^4.

I. INTRODUCTION

Two experimental techniques have been proposed and developed over decades of scientific research to determine the charge radius of the proton R_p (see Refs. [1,2] for recent reviews): the spectroscopy technique, where R_p is determined from the hyperfine structure of hydrogen atoms, and the scattering technique, where R_p is deduced from the cross section of elastic lepton scattering off a proton target. By definition, R_p is obtained from the slope of the proton electric form factor $G_E(k^2)$ at zero squared four-momentum transfer k^2,

$$R_p \equiv \sqrt{-6 \left. \frac{dG_E(k^2)}{dk^2} \right|_{k^2=0}} \tag{1}$$

which on the one hand is directly accessed from the energy levels of hydrogen atoms, and on the other hand is indirectly obtained from the measurements of $G_E(k^2)$ [3–5]. Since lepton scattering cannot reach the zero squared four-momentum transfer limit, the scattering technique relies on the zero extrapolation of $G_E(k^2)$ and then strongly depends on the functional form as well as on the data analysis method used for the extrapolation. Consequently, the scattering technique is believed to be intrinsically less accurate than the spectroscopy one. Indeed, the most precise measurements from muonic hydrogen spectroscopy 0.84184(67) fm [6] and 0.84087(39) [7] are more than ten times more accurate than the best scattering measurements 0.879(8) fm [8,9] and 0.831(14) fm [10]. This appears as a blatant limitation of the scattering technique, particularly difficult to overcome as proved by the many lepton scattering projects that developed following the advent of the so-called proton radius puzzle [11]. It also hampers any attempt to determine higher-order moments of the proton

charge density through this approach, here-after referred to as the derivative method.

The release of new hydrogen spectroscopy measurements, two within a 1σ agreement [12,13] with muonic hydrogen and one in 3.6σ disagreement [14], motivated the 2018 CODATA evaluation of the proton radius to include muonic atom data [15]. The 2018 CODATA so recommended the proton radius 0.8414(19) fm which was further confirmed within 1.6σ by a high precision measurement of the 1S-3S transition [16]. However, the latest result about the 2S-8D transition, within a 3.1σ disagreement [17] with CODATA, suggests that the issue is not yet settled.

Addressing the determination of the proton charge radius from electron scattering data, we have recently proposed a novel approach [18], referred to in the following as the integral method, that enables the determination of spatial moments of any real-valued order $\lambda > -3$ through integral forms of the Fourier transform of the probability density function. Two techniques were proposed to regularize the Fourier integrals. The weak limit one is used here for its ability to deliver analytical expressions of moments of integer order. In this approach, the λ-order moment of the proton charge spatial density $\rho_E(\mathbf{r})$ is defined as

$$(r^\lambda, \rho_E) = \langle r^\lambda \rangle = \int_{\mathbb{R}^3} d^3\mathbf{r} \, r^\lambda \rho_E(\mathbf{r}) \tag{2}$$

and can be expressed as

$$\langle r^\lambda \rangle = \frac{2}{\pi} \Gamma(\lambda + 2) \lim_{\xi \to 0^+} \int_0^\infty dk \, \mathcal{I}_\lambda(k, \xi) \, G_E(k^2) \tag{3}$$

with

$$\mathcal{I}_\lambda(k, \xi) = \frac{k \sin[(\lambda + 2) \text{Arctan}(k/\xi)]}{(k^2 + \xi^2)^{\lambda/2+1}} \tag{4}$$

TABLE I. Proton electric form factor data considered in the present study, as explained in the text.

| | | | | | k^2 range | |
Data set number	Year	Authors	Ref.	Number of data points	k^2_{min} [fm^{-2}]	k^2_{max} [fm^{-2}]
1	1962	Lehmann *et al.*	[19]	1	2.98	2.98
2	1963	Dudelzak *et al.*	[20]	4	0.30	2.00
3	1963	Berkelman *et al.*	[21]	3	25.0	35.0
4	1966	Frèrejacque *et al.*	[22]	4	0.98	1.76
5	1966	Chen *et al.*	[23]	2	30.0	45.0
6	1966	Janssens *et al.*	[24]	20	4.00	22.0
7	1971	Berger *et al.*	[25]	9	1.00	50.0
8	1973	Bartel *et al.*	[26]	8	17.2	77.0
9	1975	Borkowski *et al.*	[27]	10	0.35	3.15
10	1994	Walker *et al.*	[28]	4	25.7	77.0
11	1994	Andivahis *et al.*	[29]	8	44.9	226.
12	2004	Christy *et al.*	[30]	7	16.7	133.
13	2005	Qattan *et al.*	[31]	3	67.8	105.
14	2014	Bernauer *et al.*	[9]	77	0.39	14.2
15	2019	Xiong *et al.* - 1.1 GeV	[10]	33	5.51×10^{-3}	3.96×10^{-1}
16	2019	Xiong *et al.* - 2.1 GeV	[10]	38	1.79×10^{-2}	1.49
17	2021	Mihovilovič *et al.* - 195 MeV	[32]	6	3.43×10^{-2}	6.99×10^{-2}
18	2021	Mihovilovič *et al.* - 330 MeV	[32]	11	4.69×10^{-2}	2.00×10^{-1}
19	2021	Mihovilovič *et al.* - 495 MeV	[32]	8	1.57×10^{-1}	4.37×10^{-1}

and where the form factor and the density are related by the Fourier transform

$$G_E(k^2) = \int_{\mathbb{R}^3} d^3 r \, e^{-i k \cdot r} \rho_E(r). \tag{5}$$

The integral method overcomes the restriction of the derivative method which is limited to moments of positive even orders. Each moment order of the charge density is of interest as it carries complementary information on the charge distribution inside the proton. For instance, the short-distance behavior of the charge distribution is encoded in the negative order moments which are particularly sensitive to the large k^2 dependence of $G_E(k^2)$, while the long-distance behavior is encoded in the high positive order moments sensitive to the low k^2 dependence.

The integral method was demonstrated strictly equivalent to the derivative method for positive even order moments $\langle r^{2p} \rangle$ [18], even though basic concepts distinguish them. While the derivative method crucially depends on the way the form factor approaches its value at zero k^2, the integral method involves the full k^2 physics region as expressed by the integral in Eq. (3). This conceptual change is of importance for the determination of the functional form of $G_E(k^2)$ which can be expected more precise, and similarly for the moments. In practice the entire k^2 physics region may be restricted as the high k^2 region might not contribute significantly to the integral of Eq. (3). This is particularly true for positive order moments which, considering the k^2 dependence of experimental data, are dominated by the region $k^2 \leqslant 2$ GeV^2 (51.4 fm^{-2}).

Hence, all available data should be considered for analysis when attempting evaluations of R_p and more generally $\langle r^\lambda \rangle$. Following the formal demonstration of the integral method, the present study aims at the evaluation of a selected set of λ-order moments of the proton charge density from proton

electric form factor data, namely odd and even orders in the range $-2 \leqslant \lambda \leqslant 7$. The next section describes the selection and the analysis of experimental data. The determination of the charge density moments and of their statistical significance is discussed in a further section. A specific attention is then paid to the evaluation of the systematic errors, and is followed by a dedicated discussion on the determination of the proton charge radius in the context of the integral method.

II. ANALYSIS OF $G_E(k^2)$ EXPERIMENTAL DATA

The data inputs of the present work consist of proton electric form factor data $G_E(k^2)$ extracted from electron scattering experiments through a Rosenbluth separation [33] or for kinematical conditions where the contribution of the magnetic form factor ($G_M(k^2)$) to the cross section is strongly suppressed, for instance at very low k^2. For the purposes of the present work aiming at a quantitative evaluation of the merits of the integral method, experiments measuring polarized lepton beam observables are not considered. Consequently, $G_E(k^2)$ is overestimated at large k^2, that is in a region where it already has a small magnitude. The list of experiments selected according to the previous criteria is reported in Table I by chronological order. While modern experiments after the nineties are easily classified with respect to these criteria, the selection appears more intricate for early elastic scattering experiments where data analysis sometimes involves the empirical scaling $G_M(k^2) = \mu G_E(k^2)$ of the proton electromagnetic form factors, or where the Rosenbluth separation combines different experiments. Additionally, some analyses report negative or null squared form factors indicating some experimental issues, mostly related to a small ϵ range in the Rosenbluth separation where ϵ is the so-called polarization

TABLE II. Fit parameters of the $G_E(k^2)$ functional of Eq. (6) with their associated statistical and systematic errors.

a_1 [$\times 10^{-1}$ fm^2]	b_1 [$\times 10^{-1}$ fm^2]	b_2 [$\times 10^{-1}$ fm^4]	b_3 [$\times 10^{-3}$ fm^6]
8.8008	9.9570	1.0285	2.9252
$(\delta a_1)_{\text{Sta.}}$ [$\times 10^{-1}$ fm^2]	$(\delta b_1)_{\text{Sta.}}$ [$\times 10^{-1}$ fm^2]	$(\delta b_2)_{\text{Sta.}}$ [$\times 10^{-1}$ fm^4]	$(\delta b_3)_{\text{Sta.}}$ [$\times 10^{-3}$ fm^6]
0.0054	0.0113	0.0058	0.0666
$(\delta a_1)_{\text{Sys.}}$ [$\times 10^{-1}$ fm^2]	$(\delta b_1)_{\text{Sys.}}$ [$\times 10^{-1}$ fm^2]	$(\delta b_2)_{\text{Sys.}}$ [$\times 10^{-1}$ fm^4]	$(\delta b_3)_{\text{Sys.}}$ [$\times 10^{-3}$ fm^6]
0.0095	0.0019	0.0003	0.0219

TABLE III. Normalization fit parameters corresponding to each data set considered in this study, together with their statistical and systematic errors determined as explained in the text.

Data set number	Ref.	η_i	$(\delta \eta_i)_{\text{stat}}$ $(\times 10^{-2})$	$(\delta \eta_i)_{\text{sys}}$ $(\times 10^{-2})$
1	[19]	0.993	3.020	9.922
2	[20]	0.982	0.505	0.752
3	[21]	2.441	15.87	12.20
4	[22]	0.991	0.917	0.208
5	[23]	0.922	30.43	4.612
6	[24]	1.004	1.132	0.803
7	[25]	1.001	1.333	2.001
8	[26]	1.025	4.490	1.077
9	[27]	0.981	0.254	1.766
10	[28]	1.170	4.902	0.469
11	[29]	0.972	2.144	6.812
12	[30]	1.042	3.513	0.506
13	[31]	1.072	3.509	0.584
14	[9]	0.991	0.083	0.993
15	[10]	1.000	0.022	0.215
16	[10]	0.998	0.018	0.119
17	[32]	1.001	0.113	0.370
18	[32]	1.000	0.097	0.365
19	[32]	0.998	0.066	0.442

of the virtual photon. The reduction of the published data set following the previous criteria concerns Refs. [19,23,24], and specifically Ref. [21] for the constraint $\epsilon > 0.1$. Earlier experimental data of Refs. [34,35] were initially considered but finally rejected because of their abnormal k^2-dependence: analyzing a data set including these experiments only degrades the fit quality while not significantly changing the fit parameters. The relevant number of data points referring to a single experiment and passing the different constraints mentioned above are indicated in the fifth column of Table I. The main differences between the data sets, notably the investigated k^2-range, are reported in Table I. Note that the PRad (Proton Radius) [10] and ISR (Initial State Radiation) [32] experimental data are separated in 2 (PRad) and 3 (ISR) distinct sets corresponding to different beam energies and squared four-momentum transfer domains where the $G_M(k^2)$ contribution to the cross section is negligible.

In total, the experimental data set considered in the present study consists of 19 single electric form factor data sets up to $k^2 = 226$ fm^{-2} (8.8 GeV^2). The complete set is analyzed within a simultaneous fit approach requiring the same k^2 dependence for each of the experiments and a separate normalization parameter factor for each single data set. This is expressed in the polynomial ratio [36]

$$G_E^i(k^2) \equiv \eta_i G_E(k^2) = \eta_i \frac{1 + a_1 k^2}{1 + b_1 k^2 + b_2 k^4 + b_3 k^6}, \quad (6)$$

where η_i is the normalization fit parameter of the data set number i. Note that the use of a k^2-constant normalization parameter follows the analysis techniques of the most recent experiments [9,10,32] and remains appropriate even for high k^2 data. This k^2 region, which features form factors of very small magnitude, is of importance for the determination of negative order moments where systematic effects of the integral method dominate [18]. The results of the best fit to experimental data are reported in Tables II and III in terms of the (a_1, b_1, b_2, b_3) parameters of the form factor function and of the η_i normalization fit parameters, respectively. Statistical errors are determined taking into account the correlations between each parameter. Systematic errors of the fit parameters reflect experimental data systematics.

The systematics are determined by shifting upwards or downwards the data points of each data set with their

respective systematics. A total of 2^{19} configurations were considered, corresponding to each possible data set combination. For each configuration, the data points of a given data set are all shifted in the same direction while each data set is independently shifted upwards or downwards. The systematics on each parameter is obtained from the arithmetic average of the distribution of the difference between the parameter values of the fit of the shifted data and the ones of the reference fit in the first line of Table II.

The deviation from 1 of the normalization fit parameters of most experiments is smaller than 3% and even 1% for recent experiments [9,10,32] which have the strongest statistical weight in the fitting procedure. The renormalization of raw PRad- and A1-Rosenbluth data, as obtained from the present simultaneous fit, corrects for their incompatibility at the high k^2 end of the PRad set. A few experiments [23,28,31] feature larger deviations up to 17%, still reasonable at large k^2 where the contribution of the electric form factor to the cross section is small. Solely the experiment of Ref. [21] requires abnormally large normalization fit parameter. No experimental peculiarities have been found in this work, which may explain such a large value, but the deviation of the corresponding data points from the global trend of other experiments is particularly striking in Fig. 1 which shows the best fit (Table II) to experimental data.

This best fit accounts for a reduced χ_r^2 of 1.97, which is reasonable considering the actual dispersion of data. The residual deviation $\Delta G_i(k^2)$ of experimental data from the data set i can be defined as

$$\Delta G_i(k^2) = \frac{G_E^i(k^2) - \eta_i G_E(k^2)}{\delta G_E^i(k^2)}, \quad (7)$$
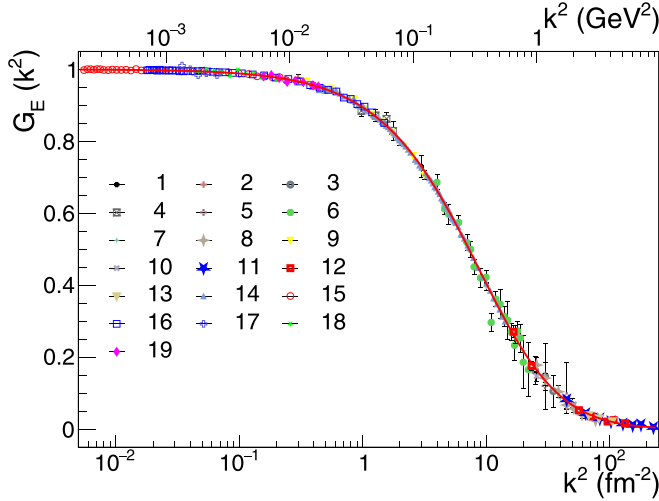
FIG. 1. Simultaneous fit (black line) of normalized experimental data $(G_E^i(k^2)/\eta_i)$ considered in Table I using the polynomial ratio function of Eq. (6). Experimental data are labeled according to the numbering of the data set (see Table I).

where $G_E^i(k^2)$ is the experimental data of the set i with its corresponding statistical error $\delta G_E^i(k^2)$ and normalization fit parameter η_i, and $G_E(k^2)$ is the fit predicted value. The distribution of $\Delta G_i(k^2)$ (Fig. 2) appears consistent with the obtained χ_r^2 value, that is in the acceptable $\pm 3\delta G_E^i(k^2)$ range.

III. DETERMINATION OF EXPERIMENTAL MOMENTS

The spatial moments of the proton charge density are determined from the form factor function using the integral method restricted to the measured physics region. This is expressed in terms of truncated moments, where the integral region of
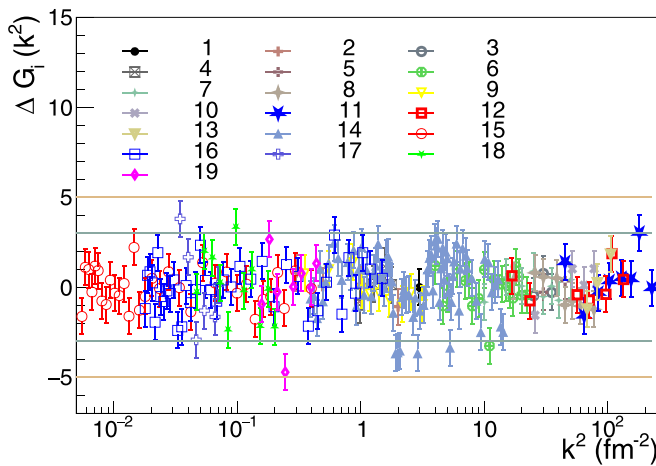

FIG. 2. Residual deviations of experimental data with respect to the fit predicted value considering their corresponding normalization fit parameter, as defined in Eq. (7) in units of the statistical standard deviation of each data point. The ± 3 and ± 5 standard deviation limits are indicated by horizontal lines. Data labels are identical to Fig. 1.

Eq. (3) is limited to a finite upper boundary Q, that is

$$\langle r^\lambda \rangle_Q = \frac{2}{\pi}\,\Gamma(\lambda+2)\lim_{\xi\to 0^+}\int_0^Q dk\,\mathcal{I}_\lambda(k,\xi)\,G_E(k^2). \qquad (8)$$

The full or infinite moment of order λ can thus be formally expressed as

$$\langle r^\lambda \rangle = \lim_{Q\to\infty}\langle r^\lambda \rangle_Q. \qquad (9)$$

In the absence of experimental data at very large k^2, perturbative quantum chromodynamics provides scaling rules which predict a rapid decrease of $G_E(k^2)$ [37]. Thus, the effect of the truncation of the integral in Eq. (8) can be controlled. The integration cut-off $Q = 7.2\,\text{fm}^{-1}$ (corresponding to $Q^2 = 51.4\,\text{fm}^{-2} = 2\ \text{GeV}^2$) considered in the present study was proven to only impact the evaluation of negative order moments [18]. Assuming a physically acceptable functional form, i.e., without any pole in the physics region, the considered form factor parametrization can be conveniently decomposed as a sum of complex monopoles according to the expression

$$G_E(k^2) = \frac{1}{b_3}\frac{1+a_1 k^2}{\left(k^2-k_1^2\right)\left(k^2-k_2^2\right)\left(k^2-k_3^2\right)}$$

$$= \sum_{n=1}^{3}\frac{A_n}{k^2+(ik_n)^2} \qquad (10)$$

with

$$A_n = -\frac{1}{b_3}\frac{1-a_1 k_n^2}{\prod_{m=1,m\neq n}^{3}\left(k_n^2-k_m^2\right)} \qquad (11)$$

and where the k_n's are the complex roots of the equation

$$(k^2)^3 + \frac{b_2}{b_3}(k^2)^2 + \frac{b_1}{b_3}k^2 + \frac{1}{b_3} = 0. \qquad (12)$$

Correspondingly, the truncated moments can be written as

$$\left(r^\lambda,\rho_{R_3^1}\right)_Q = -\sum_{n=1}^{3}\frac{A_n}{k_n^2}\left(r^\lambda,\rho_{M(ik_n)}\right)_Q, \qquad (13)$$

where the density index R_3^1 denotes the form factor parametrization with which it is Fourier related [Eq. (5)], i.e., R_3^1 stands for the ratio of a polynomial of order 1 with a polynomial of order 3 in k^2, and $M(ik_n)$ for a monopole with parameter ik_n [$\rho_{M(ik_n)} = 1/(k-ik_n)$]. The odd and even truncated monopole moments write

$$\left(r^{-2},\rho_{M(ik_n)}\right)_Q = \frac{(ik_n)^2}{2}\ln\left(1+\frac{Q^2}{(ik_n)^2}\right) \qquad (14)$$

$$\left(r^{2p-1},\rho_{M(ik_n)}\right)_Q = \frac{2}{\pi}\frac{(2p)!}{(ik_n)^{2p-1}}\left\{\text{Arctan}\left(\frac{Q}{ik_n}\right)\right.$$
$$\left.-\sum_{j=1}^{p}\frac{(-1)^j}{2j-1}\left(\frac{ik_n}{Q}\right)^{2j-1}\right\}$$
$$\qquad (15)$$

$$\left(r^{2p},\rho_{M(ik_n)}\right)_Q = \frac{(2p+1)!}{(ik_n)^{2p}}. \qquad (16)$$

TABLE IV. Moments of the proton charge density as determined from the integral method and the derivative one for even moments. The truncated moments of the second column are evaluated for the cut-off $Q^2 = 52$ fm^{-2} and the infinite moments of the third column are similarly evaluated in the limit $Q \to \infty$, assuming that the large k^2 dependence of the form factor is described by Eq. (6). Even moments obtained by the derivative method are presented in the fourth column with their associated statistical errors in the sixth column. The different systematic error labels tag their origin: the data (Dat.), the integral method (Int.), the functional form (Fun.), the data normalization parameters (Nor.), and the fitting model (Mod.) as described in the text.

				Statistical error		Systematic error				
λ	$\langle r^\lambda \rangle_Q$ [fm$^\lambda$]	$\langle r^\lambda \rangle$ [fm$^\lambda$]	$\langle r^{2p} \rangle_d$ [fm$^\lambda$]	$\delta[\langle r^\lambda \rangle_Q]$ [fm$^\lambda$]	$\delta[\langle r^{2p} \rangle_d]$ [fm$^\lambda$]	Dat. [fm$^\lambda$]	Int. [fm$^\lambda$]	Fun. [fm$^\lambda$]	Nor. [fm$^\lambda$]	Mod. [fm$^\lambda$]
-2	6.5245	8.7226	–	0.0172	–	0.0106	2.1981	0.0001	0.0095	0.3731
-1	1.9681	2.0906	–	0.0024	–	0.0019	0.1225	0.0001	0.0029	0.0278
1	0.7206	0.7179	–	0.0020	–	0.0025	0.0027	0.0001	0.0011	0.0029
2	0.6937	0.6937	0.6937	0.0094	0.0105	0.0111	0	0.0001	0.0010	0.0116
3	0.8697	0.8701	–	0.0457	–	0.0494	0.0004	0.0007	0.0013	0.0633
4	1.4728	1.4728	1.4728	0.2461	0.2365	0.2474	0	0.0065	0.0022	0.3805
5	3.8139	3.8137	–	1.4822	–	1.4297	0.0002	0.0343	0.0056	2.6276
6	16.405	16.405	16.405	10.058	10.839	9.4985	0	0.1871	0.0240	21.531
7	104.64	104.64	–	76.676	–	71.727	0.0001	2.8169	0.1528	212.48

The truncated moments corresponding to the form factor function of Eq. (6) are reported in Table IV, together with their asymptotic or so-called infinite value corresponding to the limit $Q \to \infty$. Note that the zeroth-order moment is 1 by definition of the fit function. As expected, negative moments are the only ones to significantly suffer from the truncation of the moment integral. Positive even moments are also compared to their values as obtained through the derivative method, determined from the expression

$$\langle r^{2p} \rangle_d = (-1)^p \frac{(2p+1)!}{p!} \left. \frac{d^p G_E(k^2)}{d(k^2)^p} \right|_{k^2=0}. \quad (17)$$

As demonstrated in Ref. [18], the derivative and integral determination of even moments must provide the same value, that is

$$\langle r^{2p} \rangle = \langle r^{2p} \rangle_d. \quad (18)$$

This extends to truncated moments of any form factor function through the relation

$$\langle r^{2p} \rangle = \langle r^{2p} \rangle_Q \quad (19)$$

valid for any $Q \neq 0$ (see Appendix A). It is expressed in Eq. (16) and numerically verified in Table IV.

The statistical errors of the experimental moments are determined from the propagation of the statistical errors of the fit parameters taking into account their correlations. The evaluation is based on the generation of 5×10^4 replica parameters $P^i = (a_1^i, b_1^i, b_2^i, b_3^i)$ obtained from Gaussian distributions with mean values $\mu = (a_1, b_1, b_2, b_3)$ and covariance matrix Σ as given by the fit of $G_E(k^2)$ experimental data. Each replica is built from the relationship

$$P^i = C \cdot Z^i + \mu, \quad (20)$$

where C is the triangular matrix such that

$$\Sigma = C \cdot C^T \quad (21)$$

with C^T the transposed matrix, and $Z^i = (\tilde{a}_1^i, \tilde{b}_1^i, \tilde{b}_2^i, \tilde{b}_3^i)$ is a random set of uncorrelated parameters obtained from

Gaussian distributions with unit variances and zero means. The statistical errors reported in Table IV correspond to the width of the distribution of replica moments.

The magnitude of the statistical error limits the significance of the moments determination to $\lambda < 6$. This is a consequence of the existing data set which lacks measurements at ultra low k^2. High order positive moments indeed probe the long distance behavior of the charge density and are therefore specifically sensitive to this region. High accuracy measurements in this region are extremely challenging. Concerning positive even moments, statistical errors of truncated moments can also be compared to those of the moments obtained from the derivative method. Considering the functional determined from the large data set selected in this study, the derivative method provides similar statistical errors as the integral method. As expected, the statistical uncertainty is obviously much better than the one that could be obtained from one single experiment.

IV. EVALUATION OF SYSTEMATIC ERRORS

The study developed hereafter intends to obtain as precise and realistic as possible the determination of systematic errors of the moments, a feature of upmost importance especially in the context of the proton radius determination. Five different sources of systematics are considered: the one related to the systematic error of the form factor measurements (Dat. in Table IV), the one related to the determination method of the moments (Int. in Table IV), the one intrinsic to the fit function (Fun. in Table IV), the one related to the data normalization parameters of the fit function (Nor. in Table IV), and a last one attached to the choice of the fit function (Mod. in Table IV).

The only experimental source of systematics corresponds to the error on the moment originating from the systematic errors of the measurements. It propagates to the moments through the systematics of the fit parameters and is determined by shifting upwards or downwards each parameter value with its systematic error. This leads to 2^4 possible shifted

parameter configurations for which the corresponding moments are determined and compared to the unshifted reference value. The error reported in the seventh column of Table IV is the arithmetic average of the single difference evaluations.

The other systematics are specifically attached to the integral method, i.e., do not have an experimental origin *per se*. The first of them corresponds to the under- or overestimation of the moments due to the truncation of the form factor integral. It is obtained from the comparison of the infinite (third column of Table IV) and truncated moments (second column of Table IV) and is reported in the eighth column of Table IV. The second is the error intrinsic to the fit function, that is the bias generated on the fit parameters from the model itself. The error evaluation method consists in generating form-factor pseudodata at the exact k^2 of experimental data but with a form factor value centered on the fit value $G_E(k^2)$. Each pseudodata is then distributed according to a Gaussian with variance corresponding to the statistical error of real data. The resulting pseudodata set is fitted with the function of Eq. (6) to provide new parameters that are used to compute truncated moments. The procedure is repeated 5×10^4 times to generate the distributions of the moments from pseudodata sets whose mean values are compared to the real data moments to yield the fit function systematics reported in the ninth column of Table IV. The third source of nonpurely experimental systematic is attached to the normalization of experimental data (Table III). It corresponds to the bias induced by the hypothesis that each data set may suffer from a global normalization issue as expressed by the η_i parameters. The impact of this hypothesis on the determination of density moments is evaluated by comparing the n-order reference moments of the second column of Table IV ($M_{\text{ref.}}^n$) with the average of the moments of each original data set ($\overline{M^n}$) defined as

$$\overline{M^n} = M_{\text{ref.}}^n \frac{\sum_{i=1}^{19} \eta_i \left[(\delta\eta_i)_{\text{stat}}^2 + (\delta\eta_i)_{\text{sys}}^2 \right]^{-1}}{\sum_{i=1}^{19} \left[(\delta\eta_i)_{\text{sys}}^2 + (\delta\eta_i)_{\text{sys}}^2 \right]^{-1}}. \tag{22}$$

The difference $|\overline{M^n} - M_{\text{ref.}}^n|$ is reported in the tenth column of Table IV.

The last source of systematics originates from the fitting model. The choice of the mathematical formulation of the fit function has indeed an impact on the determination of the moments [38]. The evaluation of this systematics may however suffer from bias. One may try different fit functions and select the one *best* reproducing the experimental data, in which case the model systematics is zero independently of the bias in the definition of the *best* fit. Another approach is followed here where a candidate fit to experimental data is defined as any fit function featuring $\chi_r^2 \leqslant 1.97$, that is a χ_r^2 equivalent to that of the reference fit. Several functional forms were investigated: polynomial of different orders, inverse polynomial of different orders, ratio of polynomials of different orders, and constant fraction expansion with different number of parameters. The only functions passing the selection criteria are the inverse polynomial of order 2 in k^2 and a constant fraction expansion with three or six parameters. The error reported in the eleventh column of Table IV is the difference between the average moments extracted from the functions passing the

TABLE V. Evolution along the years of the proton charge radius value as a function of the group of data sets considered for each time period.

Time period	Data set range	R_p [fm]	$(\delta R_p)_{\text{Sta.}}$ [fm]	$(\delta R_p)_{\text{Sys.}}$ [fm]
1962–1994	1–11	0.9081	0.0178	0.1249
1962–2005	1–13	0.8813	0.0191	0.1044
1962–2014	1–14	0.8837	0.0148	0.0544
1962–2019	1–16	0.8329	0.0057	0.0102
1962–2021	1–19	0.8329	0.0056	0.0097

selection criteria and the reference moments (second column of Table IV).

Except for negative moments where truncation effects are dominant, the model choice is a significant contribution to systematic errors of the integral method. It is worth noticing that this error is sometimes omitted, particularly in some of the many analyses of experimental data aimed at the determination of the charge radius of the proton after the highlighting of the proton radius puzzle [11]. Using a mathematical function obtained from a physics model is the only way to minimize this error.

V. DETERMINATION OF THE PROTON CHARGE RADIUS

As stressed in Sec. III and experimentally verified in Table IV, the integral method is strictly equivalent to the derivative method for even order moments. Particularly, we have for the second order moment

$$\langle r^2 \rangle = \langle r^2 \rangle_\varrho = -6 \left. \frac{dG_E(k^2)}{dk^2} \right|_{k^2=0}, \tag{23}$$

which, through the integral representation [Eq. (8)] of the derivative, provides a novel way for the determination of the proton charge radius from experimental data. It is instructive to look at the evolution of the R_p value over the years. Different groups of data sets are considered for this purpose, starting from a reference group gathering experimental data up to 1994 and then constituting new groups by successively adding new data sets. These groups are specifically defined in Table V. For each of them, the complete fitting procedure previously described is performed again, that is, determination of the parameters of the function of Eq. (6), evaluation of statistical and systematic errors of the parameters following the method described in Sec. II, determination of the second-order moment together with its statistical error and systematics according to Secs. III and IV, respectively. The corresponding proton radius values and errors are reported in Table V.

The analysis of form factor data up to 2014 provides a proton charge radius in excellent agreement with the A1 Collaboration result [8] and with the latest determination from the A1 cross section data only [39], however with much larger systematics. It is only taking into account the PRad [10] measurements that the same analysis method yields a result within a 2σ agreement with the measurements of muonic hydrogen [6,7]. It is worth noticing that all these evaluations of R_p, from
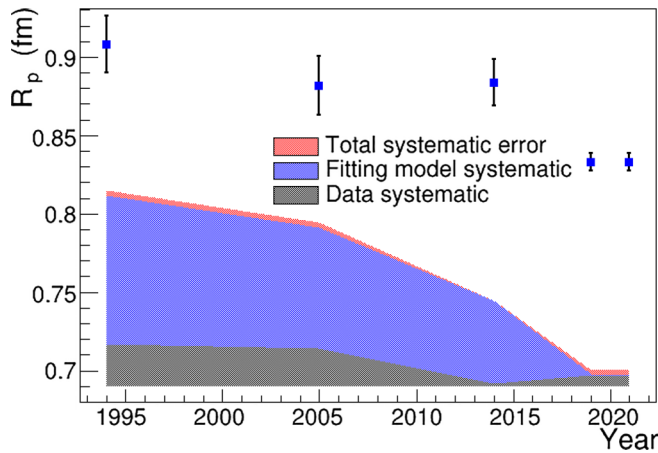
FIG. 3. Evolution of the proton charge radius value as determined with the integral method, considering the different groups of data sets defined in Table V. Each R_p point is reported at the publication year of the last data set. Error bars are only statistical, and the magnitude of systematics is indicated by the shaded bands.

early to the most recent experiments, are consistent with each other once systematic errors are taken into account.

The main sources of systematics are represented by shaded bands in Fig. 3. The choice of the form factor function appears to be the essential contribution to R_p systematic for the groups of measurements up to 2005. Its magnitude was strongly reduced by the availability of accurate low k^2 data in 2014. It is only with the latest PRad data that systematics become dominated by the component attached to experimental data. The present study of elastic electron scattering data allows the determination of R_p with a 0.9% accuracy, a remarkable number for electron scattering but still more than ten times less accurate than muonic hydrogen spectroscopy. The consistency within error bars of the different evaluations of R_p further suggests that an underestimation of the systematics in the previous determinations of the proton charge radius is most likely responsible for the reported disagreement of electron scattering and muonic atom spectroscopy. We finally note that the present analysis yields the proton charge radius value $0.8329 \pm 0.0056 \pm 0.0097$ fm in a 0.61σ agreement with the 2018 CODATA value [15] from atomic spectroscopy and with the latest dispersion analysis of the electromagnetic form factors of the nucleon [40].

Whether R_p could be interpreted as the *true* charge radius of the proton in a quantum sense is now a resolved issue. While it has been established that the spectroscopy and scattering techniques measure the same quantity in terms of the derivative of $G_E(k^2)$ [Eq. (1)] [4], it is now recognized that this quantity does not have a strict probabilistic interpretation because of the relativistic nature of the proton. It was further argued that for proton-like objects, where the intrinsic size is comparable to the associated Compton wavelength, a charge density distribution cannot be unambiguously defined [41]. Several prescriptions have been suggested, like the infinite-momentum approach showing that the Dirac form factor $F_1(k^2)$ might be more appropriate than $G_E(k^2)$ [4], however assimilating the proton to a disk. Another approach

proposing a new definition of the electromagnetic spatial densities also prefers the use of $F_1(k^2)$, however quantitatively differing from the infinite-momentum approach [42]. A recent work demonstrated that an unambiguous relativistic correction $([1 + k^2/4M^2]^{-1/2}$ with M the nucleon mass) to the conventional Sachs distributions should be considered to justify their interpretation as rest-frame distributions, providing a natural interpolation between the Breit frame and the infinite-momentum frame distributions [5,43]. This is consistent with earlier work advocating the same Darwin-Foldy correction $3/4M^2$ in the determination of nuclear sizes [44,45]. Based on this relativistic correction, we expressed in Appendix B the relativistic moments corresponding to the $G_E(k^2)$ function of Eq. (10). We incidentally note that the *proton radius* so obtained as $\sqrt{\langle r^2 \rangle}$ is $0.8526 \pm 0.0056 \pm 0.0097$ fm, where the first statistical error and the second systematic are determined following the methods described in the previous sections and using Eq. (B9).

VI. CONCLUSION

Based on a comprehensive analysis of the proton electric form factor data obtained from Rosenbluth separation and low k^2 measurements, the present work proposes an evaluation of the spatial moments of the proton charge density. A specific attention has been paid to the determination of statistical errors taking into account the correlations between the parameters of the form factor data fit. The actual status of experimental data allows a meaningful determination of the moments from $\lambda > -3$ up to the fifth order.

Similarly, the designation of the different sources of systematic errors and their evaluation are thoroughly studied. Within the integral method evaluation of the moments, the sensitivity to the specific mathematical expression of the form factor fit function and the actual experiment systematics are found to be the most significant contributions to the systematic error of the moments. Taking into account the fit function sensitivity appears to reconcile the different determinations of the proton charge radius. In that respect, the integral method approach yields the proton charge radius value $0.8329 \pm 0.0056 \pm 0.0097$ fm. The current analysis suggests that the precision of this result would be improved by enriching the electric form factor data set at very low k^2 and using form factor functions supported by physics models.

APPENDIX A: EVEN TRUNCATED MOMENTS

In this Appendix, we will show that the even-order moments do not depend on the truncation domain. The moments of the density function f at any integer order $n > -2$ can be

expressed as [18]

$$
(r^n, f)
$$

$$
= \frac{2}{\pi} \Gamma(n+2) \lim_{\xi \to 0^+} \xi^{n+2} \int_0^\infty dk \, \tilde{f}(k) \frac{k \, \Phi_n(k, \xi)}{(k^2 + \xi^2)^{n+2}}
\tag{A1}
$$

with

$$
\Phi_n(k, \xi) = \sum_{j=0}^{n+2} \sin\left(\frac{j\pi}{2}\right) \frac{(n+2)!}{j!(n+2-j)!} \left(\frac{k}{\xi}\right)^j
\tag{A2}
$$

and

$$
\tilde{f}(k) = \int_{\mathbb{R}^3} d^3 \boldsymbol{r} \, e^{-i\boldsymbol{k}\cdot\boldsymbol{r}} f(\boldsymbol{r}).
\tag{A3}
$$

In terms of the binomial coefficients C, Eq. (A2) can be rewritten

$$
\Phi_n(k, \xi) = \Im m\left[\sum_{j=0}^{n+2} \exp\left(i\frac{j\pi}{2}\right) C_{n+2}^j \left(\frac{k}{\xi}\right)^j\right]
\tag{A4}
$$

$$
= \Im m\left[\left(1 + i\frac{k}{\xi}\right)^{n+2}\right].
\tag{A5}
$$

Inserting Eq. (A5) into Eq. (A1), one obtains

$$
(r^n, f) = \frac{2}{\pi} \Gamma(n+2)
$$

$$
\times \Im m\left[i^{n+2} \lim_{\xi \to 0^+} \int_0^\infty dk \, \tilde{f}(k) \frac{k}{(k + i\xi)^{n+2}}\right],
\tag{A6}
$$

which can also be expressed as

$$
(r^n, f) = \lim_{Q \to \infty} (r^n, f)_Q
\tag{A7}
$$

with

$$
(r^n, f)_Q = \frac{2}{\pi} \Gamma(n+2)
$$

$$
\times \Im m\left[i^{n+2} \lim_{\xi \to 0^+} \int_0^Q dk \, \tilde{f}(k) \frac{k}{(k + i\xi)^{n+2}}\right]
\tag{A8}
$$

by inverting the Q and ξ limits. The distribution $(k + i0)^{-n-2}$ is defined for positive real numbers as [46]

$$
(k + i0)^{-n-2} = k_+^{-n-2} - i\frac{\pi}{2} \frac{(-)^{n+1}}{(n+1)!} \delta^{(n+1)}(k),
\tag{A9}
$$

where k_+^{-n-2} is the usual distribution as defined in Ref. [46] and $\delta^{(n+1)}$ is the $(n+1)$th derivative of the δ distribution. Particularly,

$$
(\delta^{(n+1)}, k\tilde{f}(k)) = (-1)^{n+1} (\delta, [k\tilde{f}(k)]^{(n+1)}),
\tag{A10}
$$

which inserted in Eq. (A8) through Eq. (A9) yields

$$
(r^n, f)_Q = \mathcal{A} \, \Im m[i^{n+2}] + \mathcal{B} \, \Im m[i^{n+1}]
\tag{A11}
$$

with

$$
\mathcal{A} = \frac{2}{\pi} \Gamma(n+2)
$$

$$
\times \left[\int_0^Q dk \frac{k\tilde{f}(k) - F(k)}{k^{n+2}} - \int_Q^\infty dk \frac{F(k)}{k^{n+2}}\right],
\tag{A12}
$$

$$
\mathcal{B} = (k\tilde{f}(k))^{(n+1)}|_{k=0},
\tag{A13}
$$

where

$$
F(k) = \sum_{j=0}^{(n-1)/2} g_j \, k^{2j+1}
\tag{A14}
$$

is the MacLaurin development of the odd function $k\tilde{f}(k)$. It is obvious from Eq. (A11) that the $\mathcal{A}$ term contributes only to odd integer moments ($n = 2p - 1$) and that the $\mathcal{B}$ term contributes solely to even integer moments ($n = 2p$), such that

$$
(r^{2p}, f)_Q = (-1)^p (k\tilde{f}(k))^{(2p+1)}|_{k=0}.
\tag{A15}
$$

This last equation establishes that even truncated moments for $Q \neq 0$ are independent of the truncation cut-off, and are consequently strictly equal to the infinite moment (r^{2p}, f) for any form factor function $\tilde{f}(k)$.

APPENDIX B: RELATIVISTIC MOMENTS

According to the prescription of Ref. [43], the moments of the nucleon charge density can be expressed in the Breit frame considering the correction factor

$$
f_{\text{rel}} = \left[1 + \frac{k^2}{4M^2}\right]^{-1/2},
\tag{B1}
$$

which takes into account the relativistic effects arising form the nucleon motion, and yields the substitution

$$
\widetilde{G}_E(k^2) = f_{\text{rel}} \, G_E(k^2).
\tag{B2}
$$

Particularly, the truncated moments of Eq. (8) becomes

$$
\langle r^\lambda \rangle_Q = \frac{2}{\pi} \Gamma(\lambda + 2) \lim_{\xi \to 0^+} \int_0^Q dk \, \mathcal{I}_\lambda(k, \xi) \, \widetilde{G}_E(k^2).
\tag{B3}
$$

We denote

$$
\tau_Q = Q^2/4M^2,
\tag{B4}
$$

$$
\tau_\Lambda = \Lambda^2/4M^2
\tag{B5}
$$

with

$$
\Lambda = ik_n,
\tag{B6}
$$

where k_n ($n = 1, 2, 3$) are the poles of the form factor function [Eq. (10)]. Following the monopole decomposition technique of Sec. III, Eqs. (14)–(16) become

$$
(r^{-2}, \rho_{M(\Lambda)})_Q = \frac{\Lambda^2}{2\sqrt{1-\tau_\Lambda}} \left\{\ln\left(\frac{1 - \sqrt{\frac{1+\tau_Q}{1-\tau_\Lambda}}}{1 + \sqrt{\frac{1+\tau_Q}{1-\tau_\Lambda}}}\right) + \ln\left(\frac{1 + \sqrt{\frac{1}{1-\tau_\Lambda}}}{1 - \sqrt{\frac{1}{1-\tau_\Lambda}}}\right)\right\},
\tag{B7}
$$

$$\left(r^{2p-1}, \rho_{M(\Lambda)}\right)_Q = \frac{2}{\pi} \frac{(2p)!}{\Lambda^{2p-1}} \left\{ \frac{1}{\sqrt{1-\tau_\Lambda}} \text{Arctan}\left(\frac{Q}{\Lambda}\sqrt{\frac{1-\tau_\Lambda}{1+\tau_Q}}\right) \right.$$
$$\left. +\sqrt{1+\tau_Q} \sum_{j=1}^{p} \frac{(-1)^{j-1}}{2j-1}\left(\frac{\Lambda}{Q}\right)^{2j-1} {}_2F_1\left(1, 1-j; \frac{3}{2}-j; -\tau_Q\right) \right\}, \tag{B8}$$

$$\left(r^{2p}, \rho_{M(\Lambda)}\right)_Q = \frac{(2p+1)!}{(\Lambda)^{2p}} \left\{ \frac{1}{\sqrt{1-\tau_\Lambda}} - \frac{(2p+1)!!}{(2p+2)!!}(\tau_\Lambda)^{p+1} {}_2F_1\left(1, p+\frac{3}{2}; p+2; \tau_\Lambda\right) \right\}, \tag{B9}$$

where ${}_2F_1(a, b; c; z)$ is the hypergeometric function.

[1] J.-P. Karr, D. Marchand, and E. Voutier, The proton size, Nat. Rev. Phys. **2**, 601 (2020).

[2] H. Gao and M. Vanderhaeghen, The proton charge radius, Rev. Mod. Phys. **94**, 015002 (2022).

[3] C. E. Carlson, The proton radius puzzle, Prog. Part. Nucl. Phys. **82**, 59 (2015).

[4] G. A. Miller, Defining the proton radius: A unified treatment, Phys. Rev. C **99**, 035202 (2019).

[5] C. Lorcé, Charge distributions of moving nucleons, Phys. Rev. Lett. **125**, 232002 (2020).

[6] R. Pohl et al., The size of the proton, Nature (London) **466**, 213 (2010).

[7] A. Antognini et al., Proton structure from the measurement of $2S - 2P$ transition frequencies of muonic hydrogen, Science **339**, 417 (2013).

[8] J. C. Bernauer et al. (A1 Collaboration), High-precision determination of the electric and magnetic form factors of the proton, Phys. Rev. Lett. **105**, 242001 (2010).

[9] J. C. Bernauer et al. (A1 Collaboration), Electric and magnetic form factors of the proton, Phys. Rev. C **90**, 015206 (2014).

[10] W. Xiong et al., A small proton charge radius from an electron–proton scattering experiment, Nature (London) **575**, 147 (2019).

[11] J. C. Bernauer and R. Pohl, The proton radius problem, Sci. Am. **310**, 32 (2014).

[12] A. Beyer et al., The Rydberg constant and proton size from atomic hydrogen, Science **358**, 79 (2017).

[13] N. Bezginov, T. Valdez, M. Horbatsch, A. Marsman, A. C. Vutha, and E. A. Hessels, A measurement of the atomic hydrogen Lamb shift and the proton charge radius, Science **365**, 1007 (2019).

[14] H. Fleurbaey, S. Galtier, S. Thomas, M. Bonnaud, L. Julien, F. Biraben, F. Nez, M. Abgrall, and J. Guéna, New measurement of the $1S - 3S$ transition frequency of hydrogen: Contribution to the proton charge radius puzzle, Phys. Rev. Lett. **120**, 183001 (2018).

[15] E. Tiesinga, P. J. Mohr, D. B. Newell, and B. N. Taylor, Codata recommended values of the fundamental physical constants: 2018, Rev. Mod. Phys. **93**, 025010 (2021).

[16] A. Grinin, A. Matveev, D. C. Yost, L. Maisenbacher, V. Wirthl, R. Pohl, T. W. Hänsch, and T. Udem, Two-photon frequency comb spectroscopy of atomic hydrogen, Science **370**, 1061 (2020).

[17] A. D. Brandt, S. F. Cooper, C. Rasor, Z. Burkley, A. Matveev, and D. C. Yost, Measurement of the $2S_{1/2}$-$8D_{5/2}$ transition in hydrogen, Phys. Rev. Lett. **128**, 023001 (2022).

[18] M. Hoballah, M. Barbaro, R. Kunne, M. Lassaut, D. Marchand, G. Quéméner, E. Voutier, and J. van de Wiele, Connecting spatial moments and momentum densities, Phys. Lett. B **808**, 135669 (2020).

[19] P. Lehmann, R. E. Taylor, and R. Wilson, Electron-proton scattering at low momentum energies, Phys. Rev. **126**, 1183 (1962).

[20] B. Dudelzak, G. Sauvage, and P. Lehmann, Measurements of the form factors of the proton at momentum transfers $q^2 < 2\,\text{fm}^{-2}$, Nuovo Cim. **28**, 18 (1963).

[21] K. Berkelman, M. Feldman, R. M. Littauer, G. Rouse, and R. R. Wilson, Electron-proton scattering at high-momentum transfer, Phys. Rev. **130**, 2061 (1963).

[22] D. Frèrejacque, D. Benaksas, and D. J. Drickey, Proton form-factors from proton observation, Phys. Rev. **141**, 1308 (1966).

[23] K. W. Chen, J. R. Dunning, A. A. Cone, N. F. Ramsey, J. K. Walker, and R. Wilson, Measurement of proton electromagnetic form factors at high momentum transfers, Phys. Rev. **141**, 1267 (1966).

[24] T. Janssens, R. Hofstadter, E. B. Hughes, and M. R. Yearian, Proton form factors from elastic electron-proton scattering, Phys. Rev. **142**, 922 (1966).

[25] C. Berger, V. Burkert, G. Knop, B. Langenbeck, and K. Rith, Electromagnetic form-factors of the proton at squared four momentum transfers between $10\,\text{fm}^{-2}$ and $50\,\text{fm}^{-2}$, Phys. Lett. B **35**, 87 (1971).

[26] W. Bartel, F. W. Busser, W. r. Dix, R. Felst, D. Harms, H. Krehbiel, P. E. Kuhlmann, J. McElroy, J. Meyer, and G. Weber, Measurement of proton and neutron electromagnetic form-factors at squared four momentum transfers up to $3\,\text{GeV}/c^2$, Nucl. Phys. B **58**, 429 (1973).

[27] F. Borkowski, P. Peuser, G. G. Simon, V. H. Walther, and R. D. Wendling, Electromagnetic form-factors of the proton at low four-momentum transfer, Nucl. Phys. B **93**, 461 (1975).

[28] R. C. Walker et al., Measurements of the proton elastic form-factors for $1\,\text{GeV}/c^2 \leqslant Q^2 \leqslant 3\,\text{GeV}/c^2$ at SLAC, Phys. Rev. D **49**, 5671 (1994).

[29] L. Andivahis et al., Measurements of the electric and magnetic form-factors of the proton from $Q^2 = 1.75\,\text{GeV}/c^2$ to $8.83\,\text{GeV}/c^2$, Phys. Rev. D **50**, 5491 (1994).

[30] M. E. Christy et al. (E94110 Collaboration), Measurements of electron proton elastic cross-sections for $0.4\,\text{GeV}/c^2 \leqslant Q^2 \leqslant 5.5\,\text{GeV}/c^2$, Phys. Rev. C **70**, 015206 (2004).

[31] I. A. Qattan et al., Precision Rosenbluth measurement of the proton elastic form-factors, Phys. Rev. Lett. **94**, 142301 (2005).

[32] M. Mihovilovič et al., The proton charge radius extracted from the initial-state radiation experiment at MAMI, Eur. Phys. J. A **57**, 107 (2021).

[33] M. N. Rosenbluth, High energy elastic scattering of electrons on protons, Phys. Rev. **79**, 615 (1950).

[34] F. Bumiller, M. Croissiaux, E. Dally, and R. Hofstadter, Electromagnetic form factors of the proton, Phys. Rev. **124**, 1623 (1961).

[35] R. M. Littauer, H. F. Schopper, and R. R. Wilson, Scattering of Bev electrons by hydrogen and deuterium, Phys. Rev. Lett. **7**, 141 (1961).

[36] J. J. Kelly, Simple parametrization of nucleon form factors, Phys. Rev. C **70**, 068202 (2004).

[37] S. J. Brodsky and G. R. Farrar, Scaling laws at large transverse momentum, Phys. Rev. Lett. **31**, 1153 (1973).

[38] X. Yan, D. W. Higinbotham, D. Dutta, H. Gao, A. Gasparian, M. A. Khandaker, N. Liyanage, E. Pasyuk, C. Peng, and W. Xiong, Robust extraction of the proton charge radius from electron-proton scattering data, Phys. Rev. C **98**, 025204 (2018).

[39] A. V. Gramolin and R. L. Russell, Transverse charge density and the radius of the proton, Phys. Rev. D **105**, 054004 (2022).

[40] Y.-H. Lin, H.-W. Hammer, and Ulf-G. Meißner, New insights into the nucleon's electromagnetic structure, Phys. Rev. Lett. **128**, 052002 (2022).

[41] R. L. Jaffe, Ambiguities in the definition of local spatial densities in light hadrons, Phys. Rev. D **103**, 016017 (2021).

[42] J. Y. Panteleeva, E. Epelbaum, J. Gegelia, and U. G. Meißner, Definition of electromagnetic local spatial densities for composite spin-1/2 systems, Phys. Rev. D **106**, 056019 (2022).

[43] Y. Chen and C. Lorcé, Nucleon relativistic polarization and magnetization distributions, Phys. Rev. D **107**, 096003 (2023).

[44] R. R. Yennie, M. M. Lévy, and D. G. Ravenhall, Electromagnetic structure of nucleons, Rev. Mod. Phys. **29**, 144 (1957).

[45] J. L. Friar, J. Martorell, and D. W. L. Sprung, Nuclear sizes and the isotope shift, Phys. Rev. A **56**, 4579 (1997).

[46] I. M. Guelfan and G. E. Chilov, *Les Distributions* (Dunod, Paris, 1962).